Comparative kinetic and energetic modelling of phyllosemiquinone oxidation in Photosystem I.

Stefano Santabarbara[1] and Giuseppe Zucchelli[1].

[1] Istituto di Biofisica, Consiglio Nazionale delle Ricerche, Via Celoria 26, 20133 Milano, Italy.

Supplementary information.

Section 1. Model involving large uphill electron transfer from PhQ_A^- *to* F_X*: Simulations of* PhQ^- *oxidation kinetics at room temperature considering different sets of microscopic parameters describing the rate constants.*

In this section of the Supplementary information we present kinetic simulations for an energetic scenario which consider large uphill electron transfer from PhQ_A^- to F_X, $\Delta G^0_{PhQ_A \rightarrow F_X}$ = +125meV, as derived from the temperature dependence investigation of Mula *et al.*[1]. This suggestion is in line with the structural model-based calculations of Ishikita and Knapp[2] from which, considering midpoint redox potential for F_X in the $-705 < E^0_{F_x} < -650$mV range, $+119 < \Delta G^0_{PhQ_A \rightarrow F_X} < 174$ meV. Afterward the same authors (**3**) reported that the E^0 of the $PhQ^-_{(A/B)} / PhQ_{(A/B)}$ redox pairs depended on the number of "crystallographic" water molecules explicitly included in the calculations. This could lead to ~100 mV down-shifts of the standard potential (**3**), thereby lowering the energetic barrier for electron transfer. The results from the computations of Ishikita and coworkers[2, 3] will be discussed in Section 2 of the Supplementary Information.

From the simulations presented in this paper (Figure 2A) we concluded that the energetic scenarios considering large positive value of $\Delta G^0_{PhQ_A \rightarrow F_X}$ are not compatible with the experimental kinetics. However, whereas all the parameters required to describe the electron transfer rates associated to PhQ_A^- and PhQ_B^- oxidation were taken directly from the study of Mula *et al.*[1] and see Table 1 for the

values), those concerning F_X oxidation were either compiled from the literature or assumed. The simulations of Figure 2A were obtained for $\lambda_{t,F_x \to F_A}$ = 0.7 eV, $\bar{\omega}_{F_x \to F_A}$ = 275 cm^{-1} (mean of $\bar{\omega}_{PhQ_A \to F_X}$ and $\bar{\omega}_{PhQ_B \to F_X}$) and $\Delta G^0_{F_X \to F_A}$ = –150 meV.

In the following, simulations are performed for different sets of these parameters.

1.1 Standard free energy of $F_X^- \to F_A$ electron transfer. Figure S1A shows the results of the kinetic simulations implemented considering $\Delta G^0_{F_X \to F_A}$ = –106 meV, taken from ref. **4**, whereas all the other parameters are as in Figure 2A (Main text). The overall kinetics of PhQ^- oxidation is described by lifetimes of 2.6 ns, 10 ns and 17 μs, giving an average lifetime of τ_{av} = 17.1 μs ($\langle\tau\rangle$=17.3 μs), which is much slower than the experimental figures. Figure S1B shows, instead, the results of simulations performed considering $\Delta G^0_{F_X \to F_A}$ = –200 meV, which is an extreme upper limit for the E^0 values of F_X and F_A from the literatures (see refs. **4-7** for a compilation of values). In this case PhQ^- oxidation kinetics are described by lifetimes of 2.5 ns, 9.9 ns and 5.3 μs, giving an average lifetime of τ_{av} = 5.0 μs ($\langle\tau\rangle$=5.3 μs), which still exceeds, by about an order of magnitude, the experimental reports. Hence, for energetic scenarios involving $\Delta G^0_{PhQ_A \to F_X}$ > 75 meV, even considering a very large thermodynamic drain from the system ($\Delta G^0_{F_X \to F_A}$) that likely exceed those encountered in PSI, there is no consistency between simulated and experimental kinetics.

1.2 Mean nuclear frequency coupled to $F_X^- \to F_A$ electron transfer. In the he simulations of Figure 2A the value of $\bar{\omega}_{F_x \to F_A}$ =275 cm^{-1}, corresponding to the average of $\bar{\omega}_{PhQ_A \to F_X}$ =173 cm^{-1} and $\bar{\omega}_{PhQ_B \to F_X}$ = 378 cm^{-1} as determined from molecular dynamics[1], was considered. Since this choice might appear arbitrary, kinetic simulations considering $\bar{\omega}_{F_x \to F_A}$ in the range 20 – 550 cm^{-1} were performed. This interval spans from a very soft mode (similar to that found to be associated to antenna chlorophylls) to a mid-high value, close to the average found by Moser and coworkers

(**8**) in a survey of electron transfer proteins. The results are presented in Figure S2. All other parameters associated with F_X^- oxidation were maintained as in Figure 2A, i.e. $\lambda_{t,F_x\to F_A}$ = 0.7 eV and $\Delta G^0_{F_X\to F_A}$ = –150 meV. Coupling with weak ($\bar{\omega}_{F_x\to F_A}$ = 20 cm^{-1}) or mid-frequency modes ($\bar{\omega}_{F_x\to F_A}$ = 150 cm^{-1}) lead to a further slowing down of the simulated PhQ^- oxidation kinetics, particularly of the population evolution of PhQ_A^- (Figure S2A and B), with respect to coupling with $\bar{\omega}_{F_x\to F_A}$ = 275 cm^{-1} (Figure 2A). When $\bar{\omega}_{F_x\to F_A}$ = 20 cm^{-1} is considered, the kinetics are described by lifetimes of 2.7 ns, 9.9 ns and 14.8 μs (Figure S2A). When $\bar{\omega}_{F_x\to F_A}$ = 150 cm^{-1} is considered, the lifetimes assume the values of 2.6 ns, 9.9 ns and 12.8 μs (Figure S2B). The slowest lifetime has a dominant contribution in PhQ^- oxidation, thereby the value of the average decay lifetime is τ_{av} = 17.6 μs for $\bar{\omega}_{F_x\to F_A}$ = 20 cm^{-1} and τ_{av} = 12.3 μs for $\bar{\omega}_{F_x\to F_A}$ = 150 cm^{-1} ($\langle\tau\rangle$ are 14.8 and 12.9 μs, respectively). Both are incompatible with the experimental data. When the larger value of $\bar{\omega}_{F_x\to F_A}$ = 550 cm^{-1} is taken into account, an acceleration of the simulated PhQ^- oxidation kinetics, which are then characterised by lifetime of 2.5 ns, 9.9 ns and 5.0 μs, giving τ_{av} = 5.0 μs and $\langle\tau\rangle$ = 5.2 μs, is obtained (Figure S2C). These values are the shortest obtained for any of the simulations considering a large uphill PhQ_A^- to F_X electron transfer. However, the slowest lifetime, which has also the largest amplitude, is at least 3 times larger than the upper value found in the experiments (~300 ns). Moreover, the simulated fastest lifetime from is too fast (~2 ns) to describe appropriately the experimental values of ~10-20 ns.

1.3 Reorganisation energy associated to the $F_X \to F_A$ electron transfer. The last parameter which remains to be tested is the value of $\lambda_{t,F_X\to F_A}$. In the simulations shown in Figure 2A, $\lambda_{t,F_X\to F_A}$ = 0.7 eV for all the reactions. This value was used in the analysis of the experimental values in ref. **1**. Yet, differently from the other parameters reported, this was not estimated either by computations or by the analysis of experimental data, rather it is assumed. A value of λ_t = 0.7 eV is reasonable since it is the most frequently encountered, based on the survey of several redox active proteins[8, 9] and was also found to successfully describe the PhQ^- oxidation in

previous kinetic modelling studies[6, 10]. Nonetheless, the choice of λ_t remains somewhat arbitrary. Therefore, for the large uphill $PhQ_A^- \rightarrow F_X$ electron transfer mode we have performed simulation considering initially $\lambda_{t,F_X \rightarrow F_A}$ = 0.5 eV (Figure S3A) and 1 eV (Figure S3B), but maintaining $\lambda_{t,PhQ \rightarrow F_X}$ = 0.7 eV, and successively using the same value of λ_t, being it either 0.5 eV (Figure S3C) and 1 eV (Figure S3D), for all the reactions considered.

For $\lambda_{t,F_X \rightarrow F_A}$ = 0.5 eV (Figure S3A) and $\lambda_{t,PhQ \rightarrow F_X}$ = 0.7 eV, the modelled PhQ^- oxidation is characterised by lifetimes of 2.2 ns, 9.8 ns and 2.0 μs from which τ_{av} = 1.8 μs ($\langle\tau\rangle$ = 1.9 μs). These lifetimes became 2.7, 9.9 ns and 130 μs, from which $\tau_{av} \cong \langle\tau\rangle$ = 130 μs, when $\lambda_{t,F_X \rightarrow F_A}$ = 1 eV (Figure S3B) and $\lambda_{t,PhQ \rightarrow F_X}$ = 0.7 eV are used. When λ_t = 1 eV (Figure S3D) is considered for all the reactions, the kinetics of PhQ^- oxidation are described by lifetimes of 44 ns, 121 ns and 135 μs, from which $\tau_{av} \cong \langle\tau\rangle$ = 135 μs. Instead, when homogeneous values of λ_t = 0.5 eV are used the lifetimes are 0.3 ns, 1.8 ns and 1.6 μs, yielding $\tau_{av} \cong \langle\tau\rangle$=1.6 μs (Figure S3C). Thus, for the relatively small value of $\lambda_{t,PhQ \rightarrow F_X}$ = 0.5 eV, the kinetic simulations for the large uphill PhQ_A^- oxidation model deviate the least from the experimental results. Still, the overall predicted PhQ^- oxidation for this set of parameters are too slow to be considered compatible with the experimental observation: the value of the slowest lifetime (~1.5 μs), which has dominant amplitude (97%), is about 5 times slower than that retrieved from the experiments, whereas the fastest lifetimes is about or over an order of magnitude faster. Moreover, the relative amplitude of fast:slow phase predicted from the simulation is too biased in favour of the slow component, while in experiments ratios between 0.3:0.7 and 0.45:0.55 for a wild type PS I reaction centres are reported.

Taken together, the kinetic simulations performed for the large uphill energetic model for PhQ_A^- to F_X electron transfer appears to be inconsistent with the experimental results, irrespectively of the choice of the parameters $\lambda_{t,(D \rightarrow A)}$, $\bar{\omega}_{F_x \rightarrow F_A}$ and $\Delta G^0_{F_X \rightarrow F_A}$. This model is, therefore, the less likely and less robust of all the propositions in the literature.

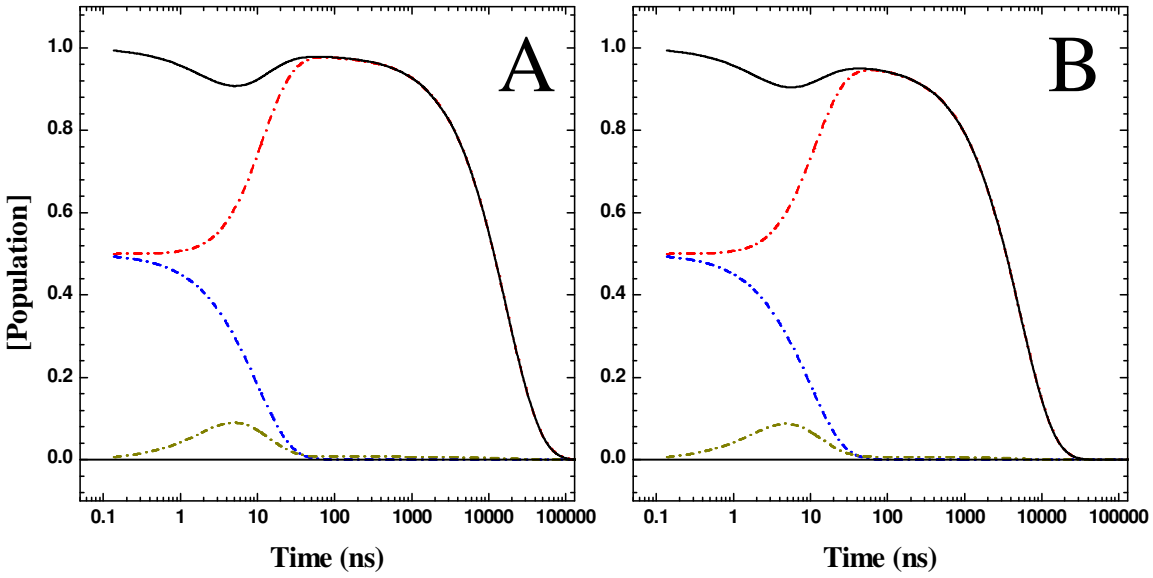

Figure S1. Kinetic simulations using the $E^0_{\mathrm{PhQ_A}}$ and $E^0_{\mathrm{PhQ_B}}$ of ref. **1**, λ_t = 0.7 eV, $\bar{\omega}_{PhQ_A \rightarrow F_X}$ = 173 cm^{-1}, $\bar{\omega}_{PhQ_B \rightarrow F_X}$ = 378 cm^{-1}, $\bar{\omega}_{F_X \rightarrow F_A}$ = 275 cm^{-1}, and two values of $\Delta G^0_{F_X \rightarrow F_A}$ equal to – 106 meV (**A**) and –200 (**B**). See text for further detail. [$\mathrm{PhQ_A^-}(t)$], dashed-dotted red-line; [$\mathrm{PhQ_B^-}(t)$], dash-dotted blue line; [$\mathrm{F_X^-}(t)$], dash-dotted golden line; [$\mathrm{PhQ_{tot}^-}(t)$], solid black line.

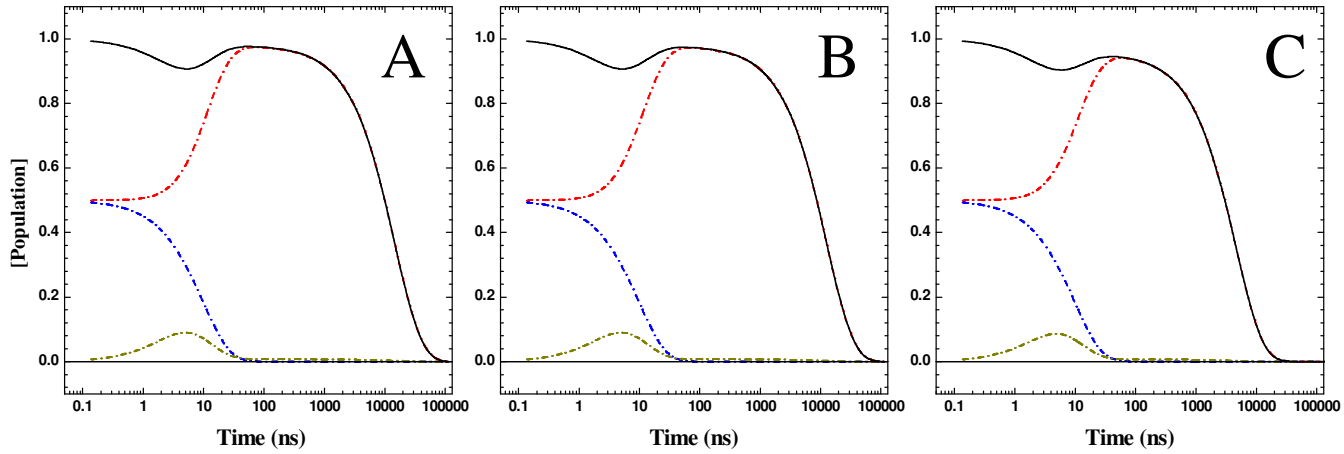

Figure S2. Kinetic simulations using the $E^0_{\mathrm{PhQ_A}}$ and $E^0_{\mathrm{PhQ_B}}$ of ref. **1**, λ_t=0.7 eV, $\bar{\omega}_{PhQ_A \rightarrow F_X}$ = 173 cm^{-1}, $\bar{\omega}_{PhQ_B \rightarrow F_X}$ = 378 cm^{-1}, and different values of $\bar{\omega}_{F_X \rightarrow F_A}$ equal to 20 cm^{-1} (**A**), 150 cm^{-1} (**B**) and 550 cm^{-1} (**C**). See text for further detail. [$\mathrm{PhQ_A^-}(t)$], dashed-dotted red-line; [$\mathrm{PhQ_B^-}(t)$], dash-dotted blue line; [$\mathrm{F_X^-}(t)$], dash-dotted golden line; [$\mathrm{PhQ_{tot}^-}(t)$], solid black line.

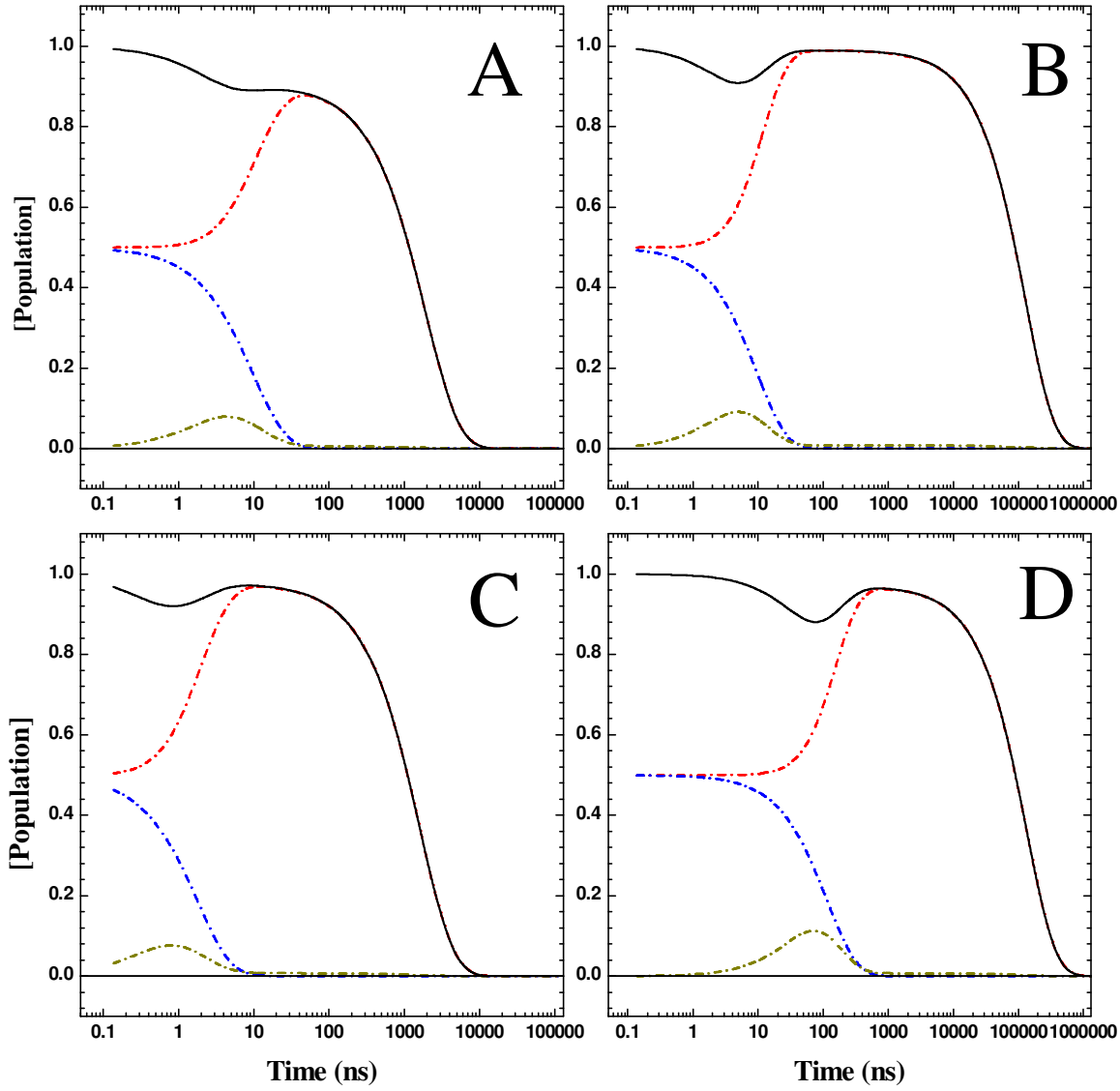

Figure S3. Kinetic simulations using the $E^0_{\mathrm{PhQ_A}}$ and $E^0_{\mathrm{PhQ_B}}$ of ref. **1**, $\bar{\omega}_{PhQ_A \to F_X}$ = 173 cm^{-1}, $\bar{\omega}_{PhQ_B \to F_X}$ = 378 cm^{-1}, $\bar{\omega}_{F_X \to F_A}$ = 275 cm^{-1}, and different values of λ_t. **A**: $\lambda_{t,F_X \to F_A}$ = 0.5, $\lambda_{t,PhQ \to F_X}$ = 0.7 eV; **B**: $\lambda_{t,F_X \to F_A}$ = 1 eV, $\lambda_{t,PhQ \to F_X}$ = 0.7 eV; **C**: $\lambda_{t,F_X \to F_A} = \lambda_{t,PhQ \to F_X}$ = 0.5 eV; **D**: $\lambda_{t,F_X \to F_A} = \lambda_{t,PhQ \to F_X}$ = 1 eV. See text for further detail. $[\mathrm{PhQ_A^-}(t)]$, dashed-dotted red-line; $[\mathrm{PhQ_B^-}(t)]$, dash-dotted blue line; $[\mathrm{F_X^-}(t)]$, dash-dotted golden line; $[\mathrm{PhQ_{tot}^-}(t)]$, solid black line.

Section 2. ***Models involving large-to-moderate uphill electron transfer from*** PhQ_A^- ***to*** F_X***:*** *Simulations of* PhQ^- *oxidation kinetics at room temperature considering different values for the standard redox potentials of* E^0 *for both phylloquinones and* F_X.

Model-based estimations of the PhQ^- standard redox potentials, other than those reported by Ptushenko *et al.*[4], were performed also by Ishikita and Knapp (**2**). The main difference between the two computation approaches is in the use of an isotropic dielectric describing the protein[2, 3], rather than different dielectric properties for the bulk and the cofactors niches[4]. Moreover, different scaling with respect to reference potential were adopted. The differences between the computational approaches and assumptions are discussed in detail in the paper of Ptushenko and coworkers[4]. It is just worth pointing out that the difference between the computed potential reported in these studies might exceed 200 mV, and is therefore significant. As noticed by Karyagina and coworkers (**3**), including a single additional water molecule observed in the structural model to the computational model can lead to shift of ~100 mV in the predicted E^0. The importance of water molecule in the vicinity of both PhQ and F_X was also discussed by Ptushenko and coworkers[4].

Here, for the sake of completeness, we limit to compare the different energetic scenarios which results from the predicted E^0 of Ishikita and coworkes[2, 3], since those suggested by Ptushenko *et al.*[4] have been already analysed in the main body of the manuscript.

Initially Ishikita and Knapp[2] indicated values of $E^0_{PhQ_A} = -531$ mV and $E^0_{PhQ_B} = -686$ mV. They compared these potentials with some of the literature report for the F_X standard potential in the range of $-705 < E^0_{F_X} < -650$ mV. This would set (+) 120 $< \Delta G^0_{PhQ_A \rightarrow F_X} <$ 174 meV, which represent a significantly uphill ET reaction. These scenarios are similar to those discussed for the parameters obtained by Mula *et al.*[1]. At the same time, the free energy for PhQ_B^- oxidation by F_X from the values of ref. **2** is $-36 < \Delta G^0_{PhQ_B \rightarrow F_X} < +19$ meV, that is, from a thermodynamic point of view, in the limit

of weakly favourable to unfavourable. This is an even lower driving force than that suggested in ref. **1**.

Kinetic simulations were performed using the $E^0_{\mathrm{PhQ_A}}$ and $E^0_{\mathrm{PhQ_B}}$ values discussed above, considering λ_t = 0.7 eV for all the reactions, $\bar{\omega}_{PhQ_A \rightarrow F_X}$ = 173 cm^{-1}, $\bar{\omega}_{PhQ_B \rightarrow F_X}$ = 378 cm^{-1} (from ref. **1**) and $\bar{\omega}_{F_X \rightarrow F_A}$ = 275 cm^{-1} (the mean of the two others), and for three values of $E^0_{\mathrm{F_X}}$ equal to –705 (Figure S4A), –670 (Fig. S4B) and –650 mV (Fig S4C). The simulations show clearly that these energetic scenarios involving very large uphill energy transfer for $\mathrm{PhQ_A^-}$ oxidation ($\Delta G^0_{PhQ_A \rightarrow F_X} >> 2\,k_B T$) and uphill to weak favourable driving force for $\mathrm{PhQ_B^-}$ oxidation ($\Delta G^0_{PhQ_B \rightarrow F_X} \cong \pm k_B T$) are inconsistent with the experimental results: the predicted mean $\mathrm{PhQ^-}$ oxidation lifetimes fall in the 6.4-51 μs range, with the fastest value obtained for $E^0_{\mathrm{F_X}}$ = –650 mV, that is, for the larger driving forces. Still, even in this case, the mean oxidation, as well as the value of the longest lifetime, exceeds by over an order of magnitude the experimental values.

After including an additional "crystallographic" water molecule to the calculations (**3**), the computed values became $E^0_{\mathrm{PhQ_A}}$ = –629 mV and $E^0_{\mathrm{PhQ_B}}$ = –776 mV. From these values and using $-705 < E^0_{\mathrm{F_X}} < -650$ mV, (+) $21 < \Delta G^0_{PhQ_A \rightarrow F_X} < 76$ meV and $-126 < \Delta G^0_{PhQ_B \rightarrow F_X} < -71$ meV are obtained. Therefore, in these scenarios, the driving force associated to $\mathrm{PhQ_B^-}$ oxidation is always predicted to be large and favourable, whereas electron transfer from $\mathrm{PhQ_A^-}$ to $\mathrm{F_X}$ is predicted to be energetically uphill, yet with a much reduced barrier than those discussed so far. Indeed, the smaller $\Delta G^0_{PhQ_A \rightarrow F_X}$ (for $E^0_{\mathrm{F_X}}$ = –670, –650 mV) are close to those considered for the "weak driving force" model, initially discusses in ref. **6**, and which is further analysed in the present paper.

The results of the kinetic simulations considering $E^0_{\mathrm{PhQ_A}}$ = –629 mV and $E^0_{\mathrm{PhQ_B}}$ = –776 mV (from Karyagina *et al.*[3]), $-705 < E^0_{\mathrm{F_X}} < -650$ mV and all the remaining parameters set as for Figure S4, are presented in Figure S5. For the energetic scenario resulting in the smaller driving forces ($E^0_{\mathrm{F_X}}$ = –705 mV), the

simulated kinetics (Figure S5A) of PhQ^- oxidation are described by lifetimes of 4.0, 8.3 ns and 1.3 μs, from which $\tau_{av} \cong \langle\tau\rangle$ = 1.3 μs, which still exceeds significantly the experimental results. However, considering $E^0_{F_X}$ = –670 mV (Figure S5B) and –650 mV (Figure S5C), the kinetics are described by lifetimes of 2.76, 11.9 and 424 ns, and 2.15, 14.3 and 237 ns, respectively, with mean oxidation times of 336 and 164 ns, which are, instead, compatible with the experimental results. In particular, the simulations of Figure S5C, for which $\Delta G^0_{PhQ_A \to F_X}$ = +21 meV and $\Delta G^0_{PhQ_B \to F_X}$ = –126 meV, describes rather closely the experimental kinetics but for an overestimation of fast oxidation phase velocity, indicating that probably $\Delta G^0_{PhQ_B \to F_X} \geq$ –120 meV and/or $\lambda_t \geq 0.7$ eV.

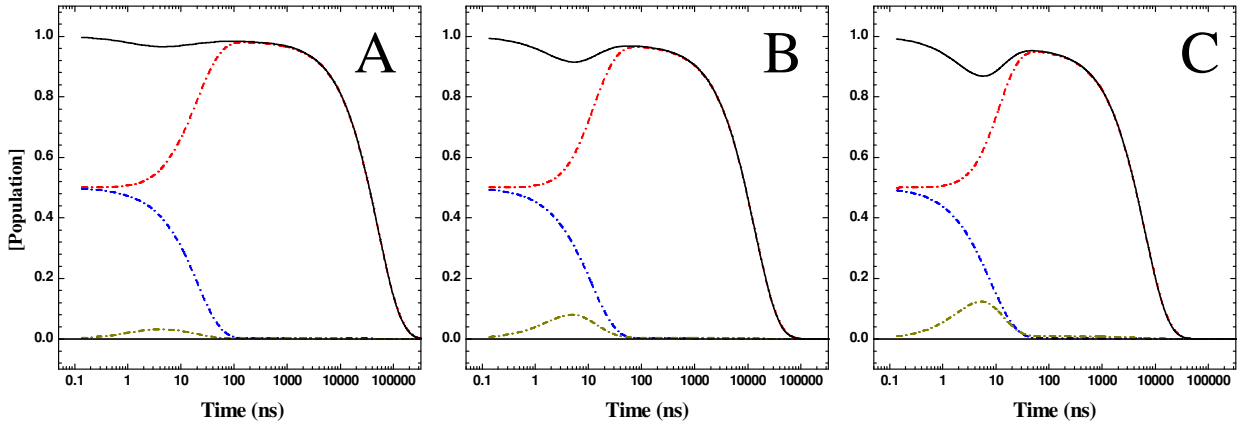

Figure S4. Kinetic simulations using the $E^0_{PhQ_A}$ and $E^0_{PhQ_B}$ of ref. **2**, λ_t = 0.7 eV, $\bar{\omega}_{PhQ_A \to F_X}$ = 173 cm^{-1}, $\bar{\omega}_{PhQ_B \to F_X}$ = 378 cm^{-1}, $\bar{\omega}_{F_X \to F_A}$ = 275 cm^{-1}, and three values of $E^0_{F_X}$ equal to –705 (**A**), –670 (**B**) and –650 mV (**C**). See text for further detail. $[PhQ^-_A(t)]$, dashed-dotted red-line; $[PhQ^-_B(t)]$, dash-dotted blue line; $[F^-_X(t)]$, dash-dotted golden line; $[PhQ^-_{tot}(t)]$, solid black line.

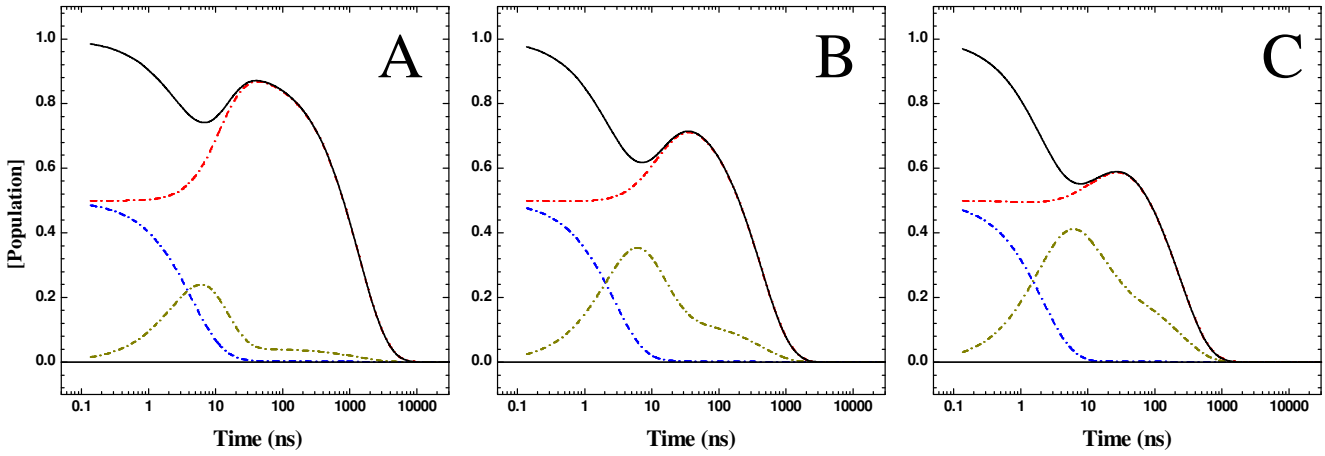

Figure S5. Kinetic simulations using the $E^0_{\mathrm{PhQ_A}}$ and $E^0_{\mathrm{PhQ_B}}$ of ref. **3**, λ_t = 0.7 eV, $\bar{\omega}_{PhQ_A \rightarrow F_X}$ = 173 cm^{-1}, $\bar{\omega}_{PhQ_B \rightarrow F_X}$ = 378 cm^{-1}, $\bar{\omega}_{F_X \rightarrow F_A}$ = 275 cm^{-1}, and three values of $E^0_{\mathrm{F_X}}$ equal to –705 (A), –670 (B) and –650 mV (C). See text for further detail. $[\mathrm{PhQ_A^-}(t)]$, dashed-dotted red-line; $[\mathrm{PhQ_B^-}(t)]$, dash-dotted blue line; $[\mathrm{F_X^-}(t)]$, dash-dotted golden line; $[\mathrm{PhQ_{tot}^-}(t)]$, solid black line.

Section 3. Temperature dependence of the rate constants of $PhQ^-_{A/B}$ ***and*** F^-_X ***oxidation.***

In the main body of the manuscript are presented the PhQ^- oxidation *lifetimes* temperature dependences, obtained by performing kinetic modelling at different temperatures. The lifetime temperature dependence is then obtained numerically since an analytical solution for the ODE system (Eqn. 1) associated to the kinetic scheme considered is not available. The lifetime temperature dependence is then determined by the individual *rate constant* temperature dependence which is simulated according to the formalism described by Eqns. (3-5).

The approach discussed above and in the text is more general than the often encountered approximation which considers that the lifetimes retrieved experimentally by fitting of kinetic traces approach the inverse of the rate constants. In fact, if the considered ET reactions were to be coupled to large driving forces, so that all the "backwards" rate constants are much smaller than the forward ones, the off-diagonal elements of matrix $\mathbf{K}$ would be small, the matrix tends to be diagonal, and the present approach converges to the usual one. However, when the off-diagonal elements are not negligible, difference might be significant so that the fitting of the lifetime by Eqn. 3-5, under the general approximation ($\tau = k_{et}^{-1}$), results in significant biased estimation of the parameters of interest.

Hence, it is more rigorous and accurate to compared the experimental results with the modelled-lifetime temperature dependences (Figures 4 and 5). At the same time, it is also interesting to compare the values of the *rates constants* temperature dependences for the two model considered compatible with the experimental results,

i.e. the weak driving force model (for) and the large driving force model. These are presented in Figure S6.

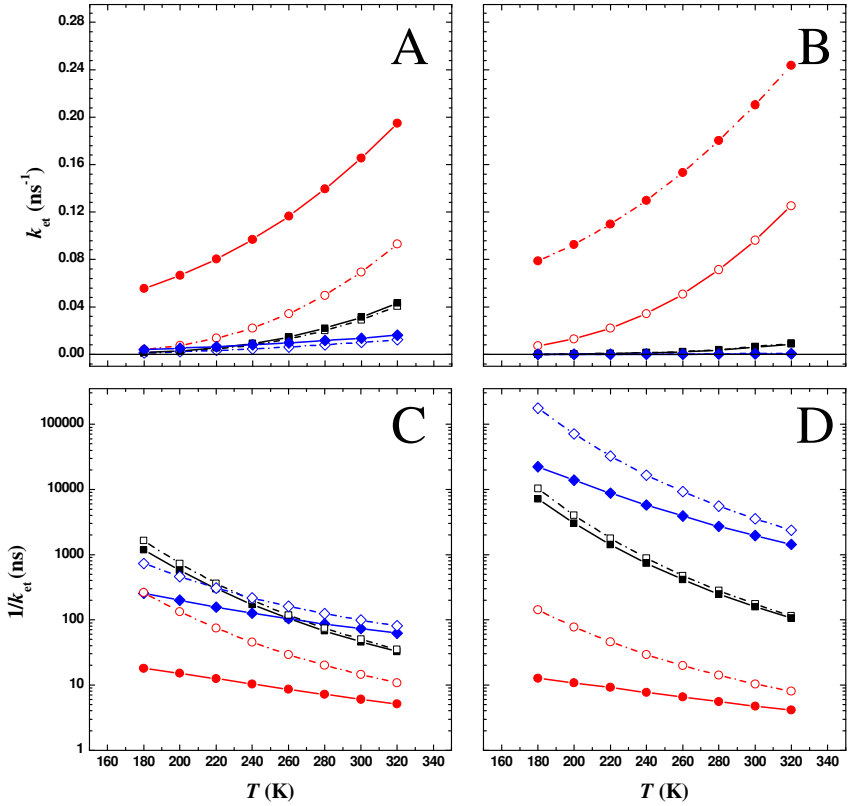

Figure S6. Temperature dependence of the rate constants of forward electron transfer, associated to PhQ_A^- (black line and symbols), PhQ_B^- (red line and symbols) *and* F_X^- (blue line and symbols) oxidation reactions. **A:** weak driving force model, considering $\Delta G^0_{PhQ_A \to F_X}$ = +10 meV, $\Delta G^0_{PhQ_B \to F_X}$ = –50 meV, $\Delta G^0_{F_X \to F_{A/B}}$ = –150 meV; λ_i = 0.7 eV and $\bar{\omega}_{D \to A}$ =150 cm^{-1} (open symbols) or $\bar{\omega}_{PhQ_A \to F_X}$ = 173 cm^{-1}, $\bar{\omega}_{PhQ_B \to F_X}$ = 378 cm^{-1}, $\bar{\omega}_{F_X \to F_A}$ = 275 cm^{-1} (closed symbols). **B**: large driving force model, considering $\Delta G^0_{PhQ_A \to F_X}$ = –86 meV, $\Delta G^0_{PhQ_B \to F_X}$ = –259 meV, $\Delta G^0_{F_X \to F_{A/B}}$ = –106 meV; λ_i = 1 eV (Open symbols) or , $\bar{\omega}_{PhQ_A \to F_X}$ = 173 cm^{-1}, $\bar{\omega}_{PhQ_B \to F_X}$ = 378 cm^{-1}, $\bar{\omega}_{F_X \to F_A}$ = 275 cm^{-1} (Closed symbols). Panels **C** and **D** shows the simulations of Figure A and B, as k_{et}^{-1} and on semi-logarithmic scale.

Figure 6A shows the lifetime temperature dependence for the weak driving force model, either considering an homogeneous value of $\bar{\omega}_{D\to A}$ = 150 cm^{-1} or asymmetric values of this parameters as indicated by molecular dynamics[1]. The lifetime temperature dependence for the large driving either considering $\bar{\omega}_{D\to A}$ = 150 cm^{-1} or the values suggested by molecular dynamics are shown in Figure 6B instead. In Figure C and D the same simulations are plotted as the inverse of the rate constant to allow direct comparison with the simulated lifetimes, shown in Figure 5 and 6.

It could be appreciated that, whereas for the large driving force model the rate constant (Figure S6D) and the lifetime (Figure 4) temperature dependences are rather similar, as expected since for this scenario the off-diagonal elements of $\mathbf{K}$ are small, for the weak driving force model the divergence is significant (Figure S6C and Figure 5) because the off-diagonal elements are not negligible. This is particularly the case for the lifetimes/rate constants describing the slowest phase of PhQ^- oxidation. In the weak driving force model, the lifetimes is determined by a significant "mixing" of rate constants, so that the oxidation of PhQ_A^- and F_X^- can not be considered as independent process, and the overall lifetime, and its temperature dependence, depends on both. Although, rigorously, this is also true for the fastest PhQ^- lifetime, the impact of rate constant mixing is less pronounced for this process.

References

1. S. Mula, M.D. McConnell, A. Ching, N. Zhao, H.L. Gordon, G. Hastings, K.E. Redding and A. van der Est, *J. Phys. Chem. B.*, 2012, **116**, 14008-14016.

2. H. Ishikita and Knapp, *J. Biol. Chem.*, 2003, **278**, 52002–52011.

3. I. Karyagina, Y. Pushkar, D. Stehlik, A. van der Est, H. Ishikita, E.W. Knapp, B. Jagannathan, R. Agalarov and J.H. Golbeck, *Biochemistry*, 2007, **46**, 10804-10816.

4. V.V. Ptushenko, D.A. Cherepanov, L.I. Krishtalik and A.Y. Semenov, *Photosynth Res.*, 2008, **97**, 55 –74.

5. K. Brettel, *Biochim. Biophys. Acta – Bioenergetics*, 1997, **1318**, 322–373.

6. S. Santabarbara, P. Heathcote and M.C.W. Evans, *Biochim. Biophys. Acta – Bioenergetics,* 2005, **1708**, 283–310.

7. N. Srinivasan and J.H. Golbeck, *Biochim. Biophys. Acta – Bioenergetics*, 2009, **1787**, 1057–1088.

8. C.C. Moser and P.L. Dutton, *Biochim. Biophys. Acta*, 1992, **1101**, 171–176.

9. C.C. Page, C.C. Moser, X. Chen and P.L. Dutton, *Nature*, 1999, **402**, 47–52.

10. C.C. Moser and P .L.Dutton, P.L. in *Photosystem I: The Light–Driven Plastocyanin:Ferredoxin Oxidoreductase*, ed. J.H. Golbeck, Kluwer Academic Publishers, Dordrecht, 2006, pp. 583-594.